Automated crack detection and measurement based on digital image correlation

Journal Article

Author(s):
Gehri, Nicola (ID); Mata Falcón, Jaime (ID); Kaufmann, Walter (ID)
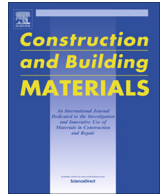
# Automated crack detection and measurement based on digital image correlation

Nicola Gehri [*,1], Jaime Mata-Falcón [2], Walter Kaufmann [3]

Institute of Structural Engineering, ETH Zürich, Switzerland

HIGHLIGHTS

- The presented procedure records the full crack behaviour in large-scale experiments.
- DIC results of the specimen's surface provide highly accurate crack measurements.
- Complex crack patters are automatically extracted using 2D image processing methods.
- Several sensitivity analyses help in understanding the measurement uncertainty.
- Crack measurements are represented with automated data visualisations tools.

GRAPHICAL ABSTRACT
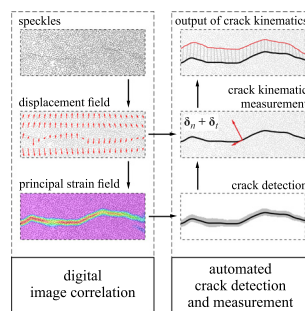
ABSTRACT

The acquisition and evaluation of the crack behaviour in experiments on quasi-brittle materials, such as concrete, mortar, or masonry is essential for understanding their structural behaviour. This publication presents a fully automated procedure to detect cracks and measure crack kinematics in laboratory experiments instrumented with digital image correlation (DIC). Crack lines are extracted using well-established image processing methods showing excellent agreement with the physical crack pattern. In contrast to most existing crack detectors that rely on pixel intensities of true images, the presented crack detection is based on the DIC principal tensile strain field what allows the extraction of much finer cracks and more reliable crack locations. The crack widths and slips are measured using the DIC displacement field accounting for local rotations of the specimen. Additionally, automated visualisations of the crack kinematic measurements including data smoothing are presented. Several sensitivity analyses evaluating the performance and the uncertainty of the crack detector and the crack kinematic measurements have been conducted. These analyses show that the obtained results depend on the DIC configuration and that the procedure is limited in the case of very closely spaced cracks. With appropriate DIC parameters, the procedure allows detecting crack locations with high precision and measuring crack kinematics very accurately even in large-scale experiments with complex crack patterns.

1. Introduction

While knowledge on the design of conventionally reinforced concrete structures is well developed, there is a rising need and interest in the assessment of existing structures as well as in the use of non-conventional reinforcement, such as fibre or textile

* Corresponding author at: Franscini-Platz 5, 8093 Zurich, Switzerland.
   E-mail address: gehri@ibk.baug.ethz.ch (N. Gehri).
[1] ORCID: 0000-0002-0321-7446.
[2] ORCID: 0000-0001-8701-4410.
[3] ORCID: 0000-0002-8415-4896.

Nomenclature

$\mathbf{a_1},\mathbf{a_2},\mathbf{b_1},\mathbf{b_2}$	position vectors in the undeformed state
$\mathbf{a_1'},\mathbf{a_2'},\mathbf{b_1'},\mathbf{b_2'}$	position vectors in the deformed state
d_1	separation distance of the two kinematic points
d_2	separation distance between the rotation and the kinematic point
f	strain filter size (defined in number of measuring points)
iw	crack inclination window size (defined in number of measuring points)
n, t	local crack coordinates
ss	subset size (in pixels)
st	step size (in pixels)
x, z	global DIC coordinates in the measuring plane
A_1,B_1	kinematic points
A_2,B_2	rotation points

O	crack point location
$\mathbf{I_2}$	identity matrix of size 2
$\mathbf{R_A},\mathbf{R_B}$	rotation matrices of crack sides A and B, respectively
T_{ε_1}	threshold of high strain areas
$\boldsymbol{\alpha}_r$	crack displacement direction
$\boldsymbol{\delta}$	crack displacement vector
$\boldsymbol{\delta_A},\boldsymbol{\delta_B}$	crack lip displacement vectors
$\boldsymbol{\delta_{A_1}},\boldsymbol{\delta_{A_2}},\boldsymbol{\delta_{B_1}},\boldsymbol{\delta_{B_2}}$	displacement vectors of the reference points
δ_n	crack opening
δ_t	crack sliding
ε_1	principal tensile strain
θ_r^0	crack inclination in the undeformed state
θ_r	crack inclination in the deformed state
$\Delta\theta_r$	mean local rotation of the crack point location
$\Delta\theta_{r,A},\Delta\theta_{r,B}$	rotation of crack sides A and B, respectively

reinforcement and digital fabrication methods [1,2]. Many mechanical models have been proposed for these materials [3–7], however, most of them lack direct experimental validation and are maybe biased by the need to interpret the measured data [8]. Novel instrumentation techniques allowing distributed measurements on the surface of and inside the structures have recently been developed [9]. They provide much more detailed measurements that reduce or even avoid the interpretation needed when selective information is measured using conventional technologies. These techniques have great potential to provide a better understanding of many mechanical phenomena on which there is still no consensus in the research community. A key aspect in understanding the structural response of quasi-brittle materials, such as concrete, mortar, or masonry, is the knowledge of crack mechanisms. Most models, codes, and standards rely on characteristic crack properties at the surface (width, slip, spacing, inclination, length, etc.), sometimes taking into account through-thickness variations with additional parameters [10]. For the validation and further development of sound structural mechanical models, surface crack measurements that allow several measurement stages are required in most cases. This paper focuses on the automated acquisition and evaluation of the crack behaviour using digital image correlation, one of the most significant novel instrumentation techniques for the non-invasive measurement of full-field surface deformations, which is currently establishing itself in many research areas.

The oldest but still much acclaimed crack measurement technique consists of visual inspection in which crack patterns are marked by eye inspection and the width of selected cracks are estimated by visual comparison with printed line-widths (magnifiers or crack loupes are used in certain cases to improve the resolution of the measurement). For predefined crack locations, usually in experiments dealing with isolated structural phenomena, demountable mechanical strain gauges (DEMEC, [11]) can be used to increase the accuracy of crack width measurements. This technique uses pre-installed discrete targets at test-specific locations on the specimen's surface, whose variation of relative distances are tracked. By arranging these targets in a grid, cracks with a priori unknown locations can also be measured. This also allows measuring crack sliding and compressive strains. However, these manual techniques are prone to measurement errors and time-consuming, which can affect the test procedure and also the structural behaviour in cases of loading rate dependencies. In addition, measurements at (or close to) failure of elements with low deformation capacity are usually missing due to the risk involved in terms of safety for the personnel and damage to the equipment

[12]. These issues can be solved by using linear displacement sensors (e.g. linear variable differential transformers (LVTDs) or electrical strain gauges) or optical tracking systems (where the displacement of markers glued on the concrete surface are measured using an active optical tracking technology). These measurement technologies provide more accurate measurements but are still limited to spatially discrete information. In order to overcome these limitations, refined crack measuring techniques are required in experiments with more complex crack patterns.

Image-based measurements are able to extract information from surface images of structures. This instrumentation is contactless and thus only minimally affects the test setup. In terms of crack measurements, there exist direct and indirect approaches to obtain crack characteristics based on images. Direct image-based crack measurements include image processing techniques that are based on variation of greyscale or colour pixel intensities. Indirect measurements, on the other hand, rely on results generated from digital image correlation in which spatial shifts of pixels between the initial and deformed state are tracked by correlating their subsets (array of neighbouring pixels). Both approaches require high-resolution cameras for detailed crack pattern acquisition, as the image-based measurement technology depends on the sensor resolution and the physical size of the area of interest.

Extracting cracks directly based on the pixel intensities is well suited for the inspection of existing structures, since no reference measurement of the undeformed state is required. This advantage has been used by many researchers to develop automated crack detection techniques using image processing methods. Such procedures aim to gain more objectivity in the quantitative analysis compared to the visual crack identification process by eye, which is tedious and depends heavily on the specialist's knowledge and experience [12]. The standard architecture of such crack detection algorithms consist of the image acquisition, followed by preprocessing steps, crack detection methods, and crack feature extraction [13]. There exist many different direct image-based crack detectors, whose concepts are typically based on (adaptive) thresholding, morphological operations, or deep learning techniques [14–20]. After the cracks have been detected, crack features, such as length, inclination, and in some algorithms also crack width, are determined. Dare et al. [21] proposed a crack width measurement approach based on the variation of pixel intensities across cracks. Another method is provided by Shan et al. [22], where crack widths are measured based on the minimum distance of opposite crack lips extracted by edge detection algorithms. These measurements are based on pixel intensities and can achieve precisions more than an order of magnitude below the pixel size in

controlled experiments and when using appropriate methods [22]. However, the smallest detectable crack width is somewhat smaller than a pixel and can only be achieved under correct conditions; under other conditions, it takes several pixel widths to reliably detect a single crack [23]. As the crack detectors depend on the lighting conditions and require a homogeneous appearance of the uncracked areas with high contrast to the cracks, the specimen surfaces usually have to be painted in white. The paint, however, can bridge cracks of small width due to its higher deformation capacity compared to the tested material. Hence, image processing-based procedures are only adequate in cases of high magnification of single cracks and if the accuracy of crack width measurements is secondary. It is important, furthermore, that this technique does not permit crack slip measurements – which is particularly relevant, for example, in experiments on aggregate interlock [24–26] – and is therefore limited in its application.

In order to counteract the limitations of direct image-based crack measurements, digital image correlation (DIC) has lately been used to a greater extent to measure crack kinematics in laboratory experiments. This technology provides highly accurate (with noise below 1/100 pixels [9]) quasi-continuous (in time and space) surface displacement measurements that can be used for both, crack detection and crack kinematic measurements. Since the obtained crack characteristics are no longer directly based on pixel intensities but on DIC results, this method is classified as an indirect image-based crack measurement. As with all image-based technologies, the quality of such measurements depends not only on the image resolution but also on the appearance of specimen's surface, the lighting conditions, and the user carefulness. DIC results are additionally very sensitive to other environmental influences, such as vibrations or heatwaves. Nevertheless, many researchers recognised the big potential of DIC for the accurate measurement of cracks [10,27–35]. In applications where single cracks are of interest, the crack locations and kinematics are typically manually extracted, as in the cases of critical shear

[10,27–31] and bending [32–34] cracks in beam tests or in tension tests [35] of concrete elements. In these approaches, the cracks are identified by focusing either at discontinuities in the displacements or at peaks in the principal tensile strains. Usually, the crack widths (and in some methods also the crack slips) are extracted by means of manually defined virtual reference points which are located at a small distance from the crack point facing each other.

If cracks and their kinematics are manually extracted from surface deformation of DIC measurements, many useful information is lost and there might be a tendency of measuring the widest cracks at their largest openings, which biases the statistics in the case of non-uniform cracks. In order to exploit the full potential of DIC measurements and to avoid the subjectivity in selection of cracks and reference points for the crack kinematic measurements, the methodology is required to be more systematic and automated. An attempt into this direction is provided by Mündecke and Mechtcherine [36] who proposed a procedure suitable for direct tension tests. They identified cracks and measured their widths using the relative deformations in the direction of the applied tension between predefined section lines. Crack initiation was set to a relative deformation of 0.025 mm, noting that this threshold should be adjusted for other experimental setups. This approach is not able to measure crack slip and is limited to tests with cracks transverse to the measuring direction since the crack widths are directly extracted from relative one-dimensional deformations.

Ruocci et al. [37,38] proposed a similar approach in which crack points are detected by analysing independently several horizontal measuring lines (Fig. 1a). The crack points are detected at local maxima in the distribution of horizontal strains. They defined a certain threshold for each measuring line above which all strain peaks are treated as crack points. The thresholds are automatically computed as the mean value plus one standard deviation ($\mu + \sigma$) of the longitudinal strain distribution in the particular measuring line (Fig. 1b). This procedure is then repeated in all parallel measuring lines of the data set. By linking successive crack points inside user-
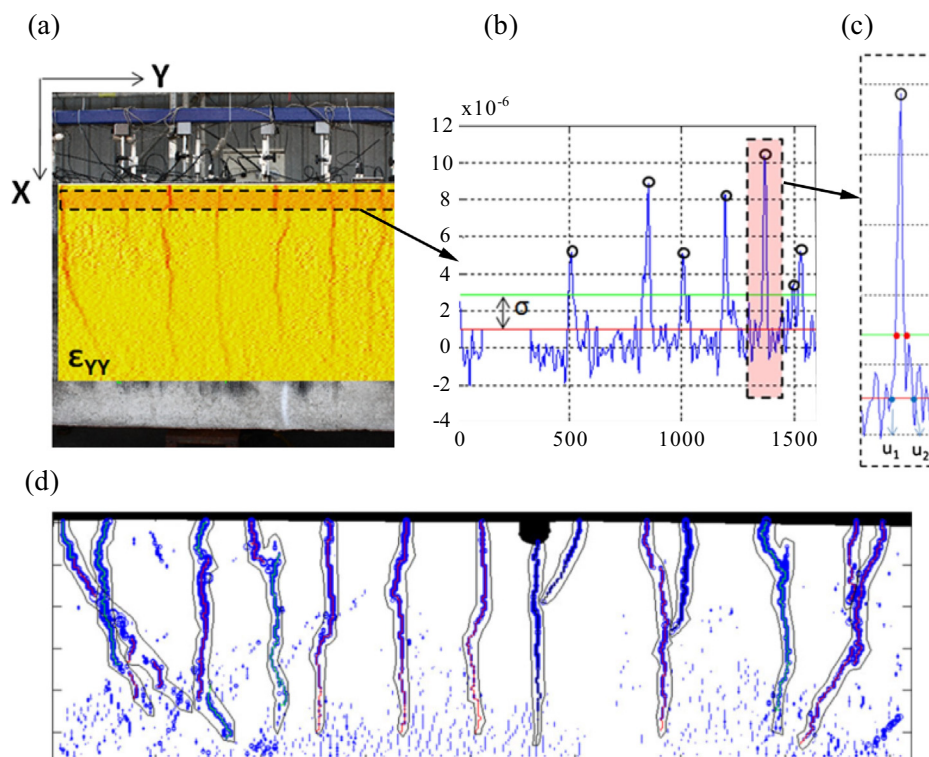

Fig. 1. Crack detection and crack kinematic measurement method proposed by Ruocci et al. [38]: (a) horizontal strain field of beam test and measuring line; (b) crack point extraction at local maxima; (c) selection of reference points for the crack kinematic measurement; (d) crack point linking within manually defined searching areas.

defined searching areas, crack paths are traced (Fig. 1d). Based on the two-dimensional surface displacement field information of two reference points at the left- and right-hand side of the crack point location (Fig. 1c), the crack widths and slips are extracted. They applied this method to beam and shear wall experiments, but did not address the underlying restrictions of the procedure when used to investigate general cracks with varying inclinations, spacings, and displacement directions: (i) the definition of the strain threshold used for the detection of crack points in a measuring line has no mechanical meaning, since the obtained value depends not only on the crack kinematics, but also strongly on the crack spacings; (ii) the crack detection method contains a direction-dependency since only longitudinal deformations are taken into account and therefore only cracks having a main opening component in the longitudinal direction can be detected; (iii) the proper extraction of crack entities by linking successive crack points is limited to cases of simple and non-branching cracks inside user-defined searching areas; and (iv) the determination of the crack displacement vector and its decomposition into crack width and slip is biased in regions with local rotations of the specimen. Even though this method for the crack detection and crack kinematics measurement is the most advanced so far, the aforementioned weaknesses strongly limits its applicability to experiments with more complex cracking behaviour.

2. Research significance

The present work proposes a fully automated crack detection and crack kinematic measurement tool for laboratory experiments instrumented with digital image correlation (DIC). DIC provides highly accurate and quasi-continuous measurements of surface displacements, allowing the detailed evaluation of the crack behaviour of quasi-brittle materials. However, existing methods to automatically extract crack locations and crack kinematics measurements from DIC results [36–38], are limited to simple crack patterns (non-branching cracks and uniform crack displacement directions) and to experiments without any rotation.

The herein presented technique addresses the strong limitations of existing methods and uses general formulations in the two-dimensional plane of the investigated surface deformations, thereby allowing to detect cracks and to measure their kinematics independent from the crack inclination and the crack displacement direction. In addition, the presented crack kinematic measurement technique is able to handle local rotations of the tested specimen, which is particularly relevant for crack slip measurements, as these are highly sensitive even to small rotations. The proposed method extracts the crack pattern as skeletons using well-established methods from image processing. This allows an accurate morphological characterisation of cracks, especially in the determination of their inclination. In contrast to the large variety of existing crack detectors, which rely on pixel intensities of true images to extract crack locations at dark pixels [12,13], the presented crack detection method relies on the DIC principle tensile strain field. Thus, the detected cracks are directly linked to the measured surface deformations, which allows the extraction of much finer cracks and more reliable crack locations.

The proposed approaches and methods provide new application possibilities, such as the accurate measurement of a complex crack behaviour in large-scale tests with varying crack inclinations and spacings and different crack displacement directions. The presented procedures are implemented in an open source software tool containing a graphical user interface that guides and supports the user in the crack selection, parameter control and the visualisation of the obtained results.

3. Description of procedure

3.1. Overview

The main concepts and steps of the automated crack detection and crack measurement (ACDM) procedure are shown in Fig. 2b. The specimen's surface is instrumented with a DIC system that tracks full-field displacements. Based on the acquired data, the principal tensile surface strain field is computed, providing the
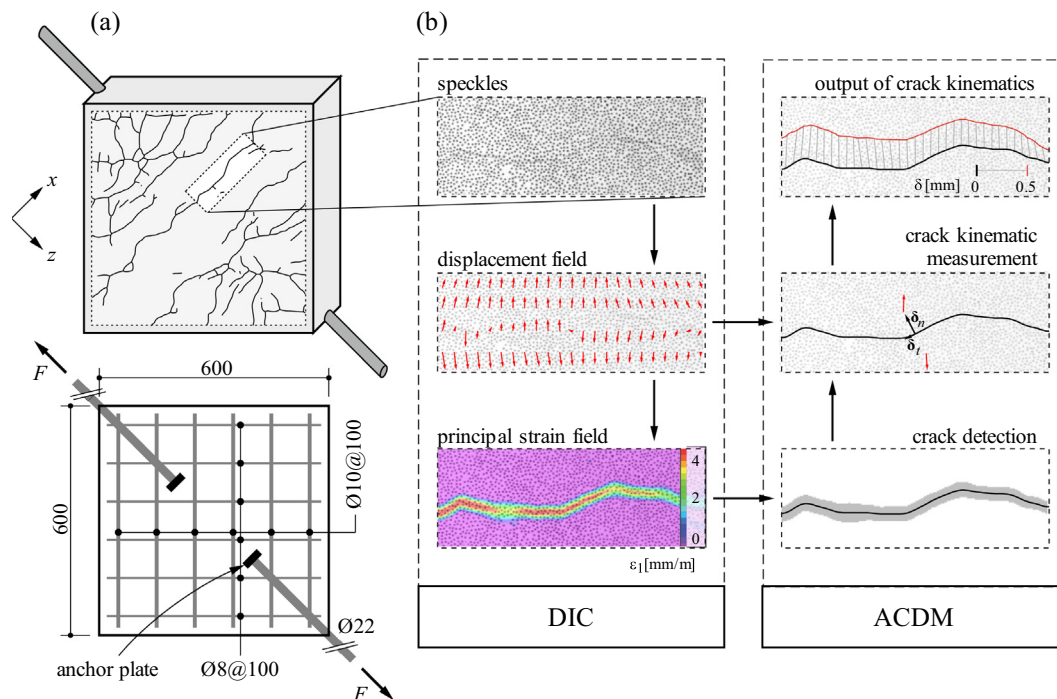

Fig. 2. Concept of the automated crack detection and crack kinematic measurement procedure: (a) setup of structural concrete experiment [39] used as test case, including the detected crack pattern; (b) flowchart of the automated crack detection and measurement (ACDM) and the DIC pre-processing steps.

input for the crack detection algorithm. Cracks are detected in areas with strains above a certain threshold. In the next step, crack entities as thinned lines connected to skeletons are extracted using morphological thinning. Finally, the crack kinematics (opening and sliding) along the crack paths are extracted. In this step, a method for determining the local crack inclination and the calculation of the relative displacements of crack lips that accounts for local rotations is used, as shown in Section 3.5. The algorithm can be applied independently to individual measuring stages or to a complete measurement series of a test where the cracks are only detected once. The entire procedure runs fully automated in an open source MATLAB tool (available at: https://gitlab.ethz.ch/ibk-kfm-public/acdm/-/releases/v1.0) and allows the user to control parameters in a graphical user interface. The following sections present the concepts and steps of the proposed crack detection and crack kinematic measurement procedure in detail.

3.2. Input data

As already introduced in previous section, the input data for the proposed procedure consists of the full-field displacement and principal tensile strain fields obtained from digital image correlation (DIC) instrumentation. It should be noted that the software tool has been developed to read DIC data generated with the software VIC-3D from Correlated Solutions Inc. [40], but could be easily be adapted to other data structures.

DIC is a novel but already well-established optical method that allows tracking the displacements of a surface based on pattern matching of digital images [41]. The main advantage of DIC compared to classical measuring techniques lies in its versatility. Since the entire surface of the specimens is monitored, the extraction of information can be tailored in the post-processing phase to the actual structural behaviour. While two-dimensional DIC applications with a single camera are restricted to measuring plane surfaces parallel to the camera sensor subjected exclusively to in-plane displacements, stereoscopic applications of DIC provide three-dimensional information and can be applied with total generality. The herein presented procedure is applicable for flat surfaces instrumented either with two- or three-dimensional DIC, however, all descriptions and measurements in this paper correspond to stereoscopic DIC instrumentation.

To track pixel displacements between the acquired images, unique correlation areas known as subsets with size ss (in pixels, see Fig. 3a) are defined in the area of interest of the images at the undeformed state. The centre of each subset (referred to as measuring point, see Fig. 3a) is tracked in each successive pair of images (deformed state) using image correlation algorithms. The measured surface is typically painted white and speckled black (see Fig. 3a) in order to minimise the noise of the subset correlation, while keeping low the size of the subset. The spacing in pixels between measuring points is referred in the following as step st (see Fig. 3a). While a measurement point can be set at every single pixel (step of one pixel), the results of consecutive pixels are not independent as the respective subsets will almost be identical. Therefore, it is common practice to set the step in the range of 1/2 to 1/3 of the subset size for standard applications [42]. However, for the purpose of the crack kinematic measurement with the procedure presented in Section 3.5 it is important to have a fine grid of independent DIC measurements. Hence, for the herein presented procedure it is recommended to use rather small subset sizes and to set the step to a very small value (in any case not larger than 1/6 of the subset size).

Once the displacements (in pixels) in each measuring point have been tracked for all images, this information is translated into global coordinates xyz by using an appropriate model of the optical
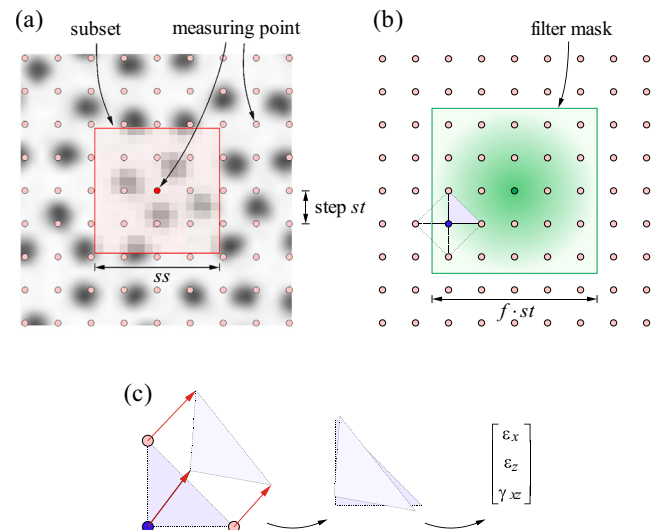

Fig. 3. DIC definitions according to [43]: (a) subset with size ss, step st, and measuring points; (b) strain filtering with rotationally symmetric centre-weighted Gaussian filter mask of size f; (c) details of strain computation.

system, based on photogrammetry principles. The optical system should be calibrated for each measurement, with the acquisition of a number of images of a rigid calibration plate containing fiducial points. It should be noted that the herein presented procedure only uses the in-plane components of the flat measuring surface despite that the displacement field is obtained three-dimensionally. This is sufficient to measure crack widths and slips (out-of-plane components of the crack kinematics are generally low and not relevant for in-plane loading). The strain field is finally computed in the post-processing from the measured displacement field, following the principles shown in Fig. 3c. A rotationally symmetric centre-weighted Gaussian filter mask is typically applied to smooth the local results of strains (see Fig. 3b). The size of the smoothing group is defined by a user-specific filter f (defined in number of measuring points).

The individual concepts of the proposed crack detection and measurement method are presented in this paper with the help of results from an experiment conducted by Häfliger et al. [39], shown in Fig. 2a. A square concrete panel with 600 mm side length, orthogonally reinforced with stirrups of diameter 10 mm and 8 mm in the particular directions, was subjected to diagonal tension F introduced by two 22 mm headed bars. The maximum aggregate size of the concrete was 16 mm. One side of the panel was instrumented with a 3D DIC system with an image resolution of 2.63 pixel/mm. The correlation was carried out with the software VIC-3D (Correlated Solutions Inc. [40]). The resulting complex crack pattern is ideal for showing the high potential of the proposed crack detection and crack kinematic measurement procedure.

3.3. Crack detection

From a mechanical point of view, surface cracks are defined as displacement discontinuities. A simple method for the automated detection of crack locations based on DIC measurements is the identification of crack points by a specific deformation onset. Cracks can also be detected relying on strains calculated from the DIC displacement field. Since the strain field of the specimen's surface has a certain resolution and is smoothed through the filter mask, the actual displacement discontinuities at cracks result in strain peaks with magnitudes related to the crack kinematics. It

should be noted that existing automated crack detection approaches are limited to extract crack points based on DIC information at one-dimensional measuring lines, either relying on longitudinal displacements [36] or strains [37,38]. However, when only using longitudinal information, cracks that open perpendicularly to the measuring line cannot be detected and the detection only yields information of independent crack points. Additionally, tracing crack paths by linking successive crack points, as proposed in [37,38] inside user-defined searching areas (see dark contours in Fig. 1d), is hardly possible to be automated for complete crack patterns with branching cracks. The direction-dependency and the restriction to simple crack patterns of such methods strongly limits their general applicability.

In order to overcome the aforementioned limitations, the herein presented crack detection approach uses two-dimensional image processing methods relying on magnitudes of principal tensile strains, thus making the crack detection direction-independent. The concept of extracting the crack pattern from the DIC principal tensile strain field is shown in Fig. 4 and consists of thresholding and morphological thinning to skeletons, with the latter being particularly important to clearly characterise and trace crack branches (see Sections 3.4 and 3.5). Using a certain threshold T_{ε_1} (which should be above the sum of the maximum elastic (uncracked) tensile strains of the material and the measurement's noise level), the principal tensile strain field is binarised into high strain areas containing the crack locations and low strain areas representing uncracked zones. Hence, the smallest detectable crack width is linked to the user-defined threshold value. Typical values of the smallest detectable crack width will be discussed in Section 4.1. The obtained high strain areas are then converted to skeletons using morphological thinning operations from MATLAB's Image Processing Toolbox [44] in order to obtain well-defined crack lines.

The proposed approach can be applied independently at individual measuring stages of a test, but (i) causes problems at high crack widths since the correlation can be locally lost near cracks – shown in Fig. 4 as white areas in the principal tensile strain fields – and (ii) results in crack patterns that can be incoherent between measuring stages. Regarding the first issue, directly performing the detection with a measuring stage containing correlation losses would lead to missing actual wide cracks and extracting fictitious cracks instead. Simply interpreting correlation losses as high strains would be inappropriate, as they might also occur in uncracked areas. Therefore, a practical solution to this issue has been implemented for the case of progressive crack formation (typically in monotonically loaded tests), consisting of detecting cracks using previous measuring stages by combining the individual binarisation of high strain areas (refer to the combining step in Fig. 4). The second issue is tackled by detecting the crack pattern only once at a measuring stage representative of the stabilised crack pattern, which is then used for the crack measurement in all measuring stages. For convenience, the crack pattern skeleton is always defined with respect to the undeformed state, whereas the deformations are considered in the calculation of the crack kinematics, as will be shown in Section 3.5. Crack initiation of each crack point is determined based on the evolution of crack kinematic quantities through the measuring stages. Compared to detecting cracks at individual measuring stages, this approach also drastically reduces computation time.

3.4. Crack characterisation

In order to analyse quantitatively cracks in terms of their geometrical and topological properties and their crack kinematics, it is essential to divide the crack pattern skeleton into individual traceable crack branches and to identify their connectivity. The crack pattern skeleton is segmented in labelled crack branches and nodes as shown in Fig. 4, using morphological filtering and segmentation operations [44]. While this procedure would also allow identifying and removing spurious unwanted small crack branches, this feature is currently not included in the software tool.

An important characteristic in the automated selection of reference points for the calculation of the crack displacement vector and its decomposition in crack width and slip (discussed in Section 3.5) is the crack inclination. The determination of the crack inclination should be carried out carefully, especially in experiments on aggregate interlock, since most models for the stresses transferred across cracks are very sensitive to small variations in the crack kinematics [24,25,45]. The crack inclination of a crack point in the undeformed state θ_r^0 is a property of the local crack line
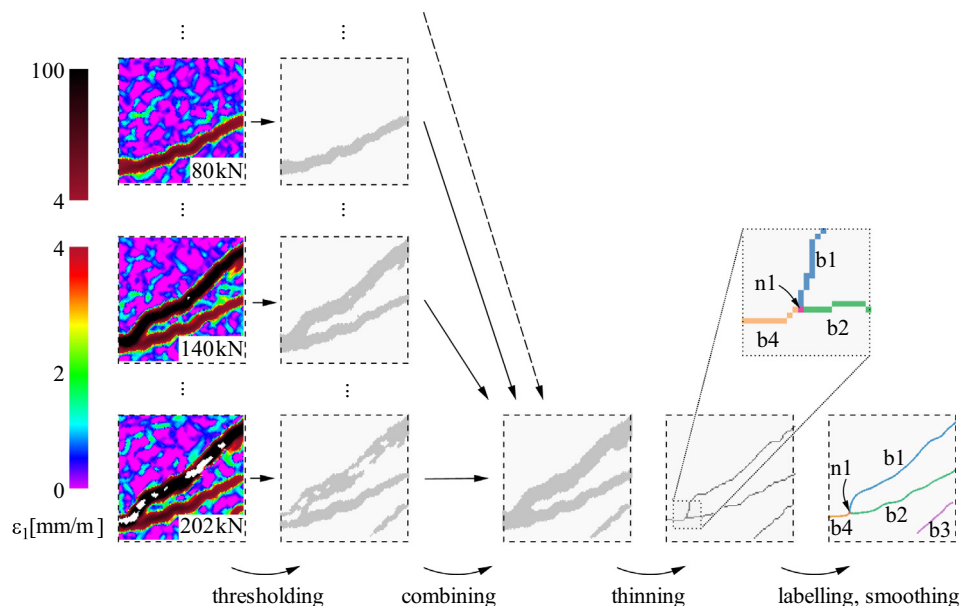

Fig. 4. Details of crack detection procedure: thresholding of principal tensile strain fields of multiple measuring stages; combining individual high strain areas; thinning to crack line skeleton using morphological operations; labelling and smoothing of crack line branches.

shape. θ_r^0 is defined on the interval $(-\pi/2, \pi/2]$ as the angle between the x-axis and the major axis of the ellipse that has the same second moment of inertia as the crack part lying within a user-defined crack inclination window of size iw (defined in number of measuring points) whose centre coincide with the particular crack point (Fig. 5c). The size of the square crack inclination window is set by the user and can affect θ_r^0 and all values dependent on it as shown in Section 4.2.

3.5. Crack kinematic measurement

Crack kinematics are the relative displacements of crack lips. Generally, when crack kinematics are extracted from DIC results, it is important to consider that displacement measurements at points whose DIC subsets intersects the crack location are biased (as will be discussed in Section 4.3). Therefore, the crack lip displacements can only be accurately measured outside the immediate vicinity of the crack locations. When manually extracting crack kinematics from DIC results, the crack lip displacements are usually defined by means of two reference points close to the crack point that are approximately perpendicular to the crack inclination and have a certain distance to each other. In such approaches, the crack inclination is typically visually determined. In the automated crack kinematic measurement method proposed by Ruocci et al. [38], the two reference points are selected at the left- and right-hand side of the crack point location. The separation of the points is defined based on the longitudinal strains (i.e. the points are located where the strains first intersect the mean strain value of the measuring line, see blue markers in Fig. 1c). While this approach implicitly attempts to avoid using biased points (i.e. points with DIC subsets intersecting the crack lines), the automatically computed separation lacks direct physical meaning and general validity.

The characterisation of a crack lip displacement by a single reference point that has a certain distance to the actual crack location and is approximately perpendicular to the crack inclination, has proven to be useful in many applications, but leads to problems in the case of local or global rotations of the specimen. Even though in most applications such rotations are rather small and therefore only minimally affect crack opening results, this effect becomes significant when measuring crack slidings even for minor rotations. In common test setups and DIC configurations, this false

crack sliding reaches several tenths of a mm per degree of specimen rotation. The herein proposed method addresses this issue and presents an automated rotation-independent crack kinematic measurement procedure, illustrated in Fig. 5.

The crack displacement vector is calculated in a similar manner to the method proposed by Campana et al. [46] for discrete surface displacement measurements performed with demountable mechanical strain gauges (DEMEC, [11]). Assuming rigid-body displacements at both crack sides A and B in the vicinity of the crack point location O, the crack lip displacements are defined with the help of four close reference points (A_1, B_1, A_2, and B_2, see Fig. 5a) in the DIC displacement field. It is noted that dealing with DIC data allows a refined and more sophisticated selection of reference points compared to the available discrete measurement point used in [46]. The reference points in the herein presented procedure are grouped into kinematic points (A_1 and B_1) and rotation points (A_2 and B_2). The kinematic points describe the rigid-body displacements of the crack sides A and B. The rotation points are explicitly used to define the rigid-body rotation of the respective crack side:

$$\Delta\theta_{r,A} = \tan^{-1}\left(\frac{\mathbf{a_2} \times \mathbf{a_2'}}{\mathbf{a_2} \cdot \mathbf{a_2'}}\right), \quad \Delta\theta_{r,B} = \tan^{-1}\left(\frac{\mathbf{b_2} \times \mathbf{b_2'}}{\mathbf{b_2} \cdot \mathbf{b_2'}}\right) \quad (1)$$

with $\mathbf{a_2}$ and $\mathbf{b_2}$ being the vectors from the kinematic points to the rotations points in the undeformed state and $\mathbf{a_2'}$ and $\mathbf{b_2'}$ the same vectors in the deformed state.

The kinematic and rotation points are selected among the available grid of measuring points to match best the following conditions: (i) the kinematic points are set perpendicular to the crack and spaced by d_1; (ii) the rotation points are set parallel to the crack and separated to the kinematic points by d_2. While small deviations of the ideal locations of these points do not affect the accuracy of the crack kinematic measurements, it is hightly recommended to use a fine grid of measuring points (obtained by computing DIC with a small step size st). For defining these points, the crack inclination in the undeformed state θ_r^0 is considered.

The crack lip displacements are then obtained using the following expressions:

$$\boldsymbol{\delta_A} = \boldsymbol{\delta_{A_1}} + (\mathbf{I_2} - \mathbf{R_A})\mathbf{a_1} \quad, \boldsymbol{\delta_B} = \boldsymbol{\delta_{B_1}} + (\mathbf{I_2} - \mathbf{R_B})\mathbf{b_1} \quad (2)$$

with

$$\mathbf{R_A} = \begin{bmatrix} \cos(\Delta\theta_{r,A}) & -\sin(\Delta\theta_{r,A}) \\ \sin(\Delta\theta_{r,A}) & \cos(\Delta\theta_{r,A}) \end{bmatrix}, \mathbf{R_B} = \begin{bmatrix} \cos(\Delta\theta_{r,B}) & -\sin(\Delta\theta_{r,B}) \\ \sin(\Delta\theta_{r,B}) & \cos(\Delta\theta_{r,B}) \end{bmatrix} \quad (3)$$

as the in-plane rotation matrices, $\mathbf{a_1}$ and $\mathbf{b_1}$ the vectors from the crack point to the kinematic points in the undeformed state, and $\boldsymbol{\delta_{A_1}}$ and $\boldsymbol{\delta_{B_1}}$ the displacements at the kinematic points. Hence, the crack displacement vector is defined as the relative crack lip displacement of side B with respect to side A as illustrated in Fig. 5b, i.e.:

$$\boldsymbol{\delta} = \boldsymbol{\delta_B} - \boldsymbol{\delta_A} \quad (4)$$

Assuming parallel crack lip planes, generally the crack displacement vector $\boldsymbol{\delta}$ is inclined by α_r with respect to the crack inclination in the deformed state

$$\theta_r = \theta_r^0 + \Delta\theta_r \quad (5)$$

where θ_r^0 is the inclination in the undeformed state with respect to the x-axis (see definition in Section 3.4) and

$$\Delta\theta_r = (\Delta\theta_{r,A} + \Delta\theta_{r,B})/2 \quad (6)$$

is the mean local rotation of sides A and B (see Fig. 5b). The decomposition of the crack displacement vector $\boldsymbol{\delta}$ into crack opening δ_n and crack sliding δ_t is conducted with the following expressions:

$$\delta_n = \sin(\alpha_r)\|\boldsymbol{\delta}\|, \delta_t = \cos(\alpha_r)\|\boldsymbol{\delta}\| \quad (7)$$
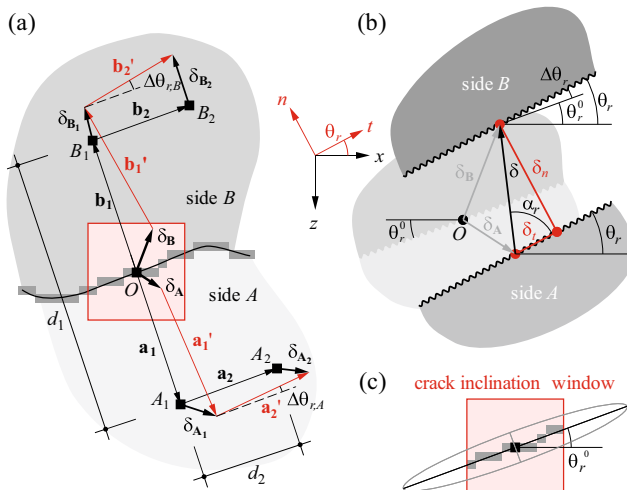

Fig. 5. Details of crack kinematic measurement: (a) crack displacement vector calculation, (b) decomposition of crack displacement vector in crack opening δ_n and sliding δ_t, (c) definition of crack inclination in the undeformed state θ_r^0.

The proposed method determines properly the crack kinematics while dealing consistently with local rotations of the specimen, as long as the reference points characterise sufficiently the crack lips displacements (i.e. if the region between the crack lip, the kinematic point, and the rotation point displaces as a rigid-body for both crack sides). This assumption of rigid-body movement can be considered fulfilled if the region is not disturbed by any crack, since the deformations in uncracked areas of quasi-brittle materials are typically much lower than the crack displacements. In Section 4.3, the limitations of the crack kinematic measurement are discussed, especially in applications with small crack spacings.

3.6. Data smoothing and visualisation

In addition to factors influencing the performance of the crack detection and measurement technique presented above, the accuracy and precision of the detected crack locations and the crack kinematic measurements is strongly dependent on the configuration and uncertainty of the DIC data and the image resolution. The quality of results can be improved by reducing the DIC noise with the help of appropriate data smoothing. This section presents several data smoothing tools that have been implemented in the herein proposed method. These tools are divided into crack line and crack kinematic smoothing operations. Additionally, several automated data visualisations are shown.

Smoothing of crack lines is explicitly used for visualisation purposes to obtain a more realistic representation of the crack line without minor local arching. It has no influence on the crack inclination nor on the crack kinematic measurements and can be easily performed by a moving average filter of the coordinates of the crack point locations. On the other hand, smoothing of crack kinematics must be conducted more carefully, since the independent smoothing of magnitudes of crack openings and crack slidings would disregard the fact that crack kinematics are direction-dependent. Therefore, the implemented crack kinematic smoothing tool filters the crack openings and slidings by means of the xz-coordinates of the crack displacement vectors. The crack kinematic smoothing can be either conducted as a time filter over several measuring stages or as spatial filter along the crack path. The spatial smoothing operation is justified by the assumption of local rigid-body movements of the crack lips.

Fig. 6 shows three automatically generated visualisations of the crack pattern and the measured crack kinematics from the panel experiment in Fig. 2a. The cracks are detected with the parameters specified in Fig. 7. The inclination window size iw is chosen equal to one maximum aggregate size of the concrete (16 mm). The crack kinematics are measured with $d_1 = d_2 = 8.1$ mm (using the minimum separation distance as will be defined in Eq. (9)) and smoothed using a moving average path filter with span 5 (which corresponds to 3.8 mm). Fig. 6a shows the crack locations and measured crack openings, magnified by factor 10, at ultimate load F_{ult}. Fig. 6b additionally indicates the local crack sliding to opening ratio by colour. These two visualisations types represent single measuring stages and mainly help to understand spatial variations of crack mechanisms. On the other hand, Fig. 6c shows a detail of the central crack indicating three different measuring stages and the evolution of crack displacement vectors (in grey) within successive stages (in red, starting with the crack initiation at $0.60 F_{ult} = 121$ kN), similarly as represented by Cavagnis et al. [27]. The crack lines are indicated in black and the crack kinematics are shown for the main crack in this window.

4. Measurement uncertainty

4.1. Performance of the crack detection

The performance of a crack detector is usually evaluated by comparing its output to the real crack pattern. In the case of direct image-based crack detectors (relying on the variation of pixel intensities), the real crack pattern is represented by an ideal result – often referred as the ground truth. This is most commonly obtained from manual labelling [47], either on images or on the specimen's surface. For the evaluation of indirect image-based crack detectors which relies on DIC information as the herein proposed method, the manual labelling of crack locations is hindered by the applied paint on the specimen's surface (cracks cannot be identified in dark speckles and the white base paint can bridge cracks of small width). The manual labelling on images cannot be used as the ground truth for the evaluation of DIC-based crack detectors in large areas: the smallest identifiable crack width when manually labelling cracks on the images is limited by the image resolution, which is usually worse compared to the one provided by DIC-based crack detectors (see Table 1.). While labelling on the specimen's surface allows identifying finer cracks, marking the surface would hinder conducting further DIC measurements, as the reference subsets would be distorted. A good alternative is the extraction of the ground truth from the DIC results by labelling crack locations using the DIC displacement or strain field. This
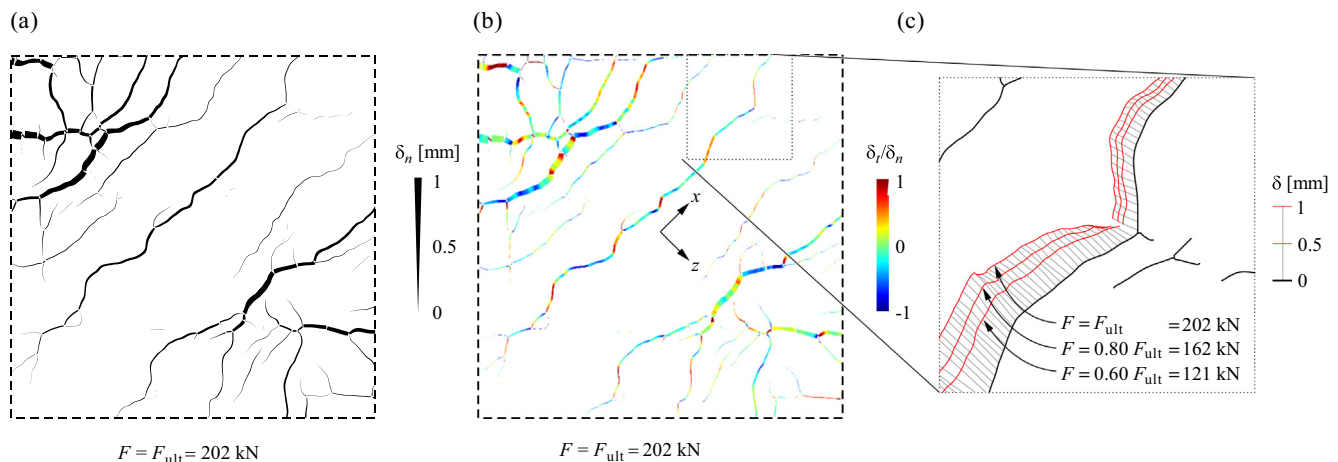

(a)

δ_n [mm]

$F = F_{ult} = 202$ kN

(b)

δ_t/δ_n

$F = F_{ult} = 202$ kN

(c)

δ [mm]

$F = F_{ult}$ = 202 kN
$F = 0.80 F_{ult} = 162$ kN
$F = 0.60 F_{ult} = 121$ kN

Fig. 6. Automated data visualisations: (a) crack pattern with crack opening measurements indicated by line width at ultimate load F_{ult} (crack opening measurements magnified by factor 10); (b) crack pattern with full crack kinematic measurement representation (colour represents crack sliding to crack opening ratio) at ultimate load F_{ult}; (c) crack displacement vectors of three successive measuring stages (crack kinematic measurements magnified by factor 100).
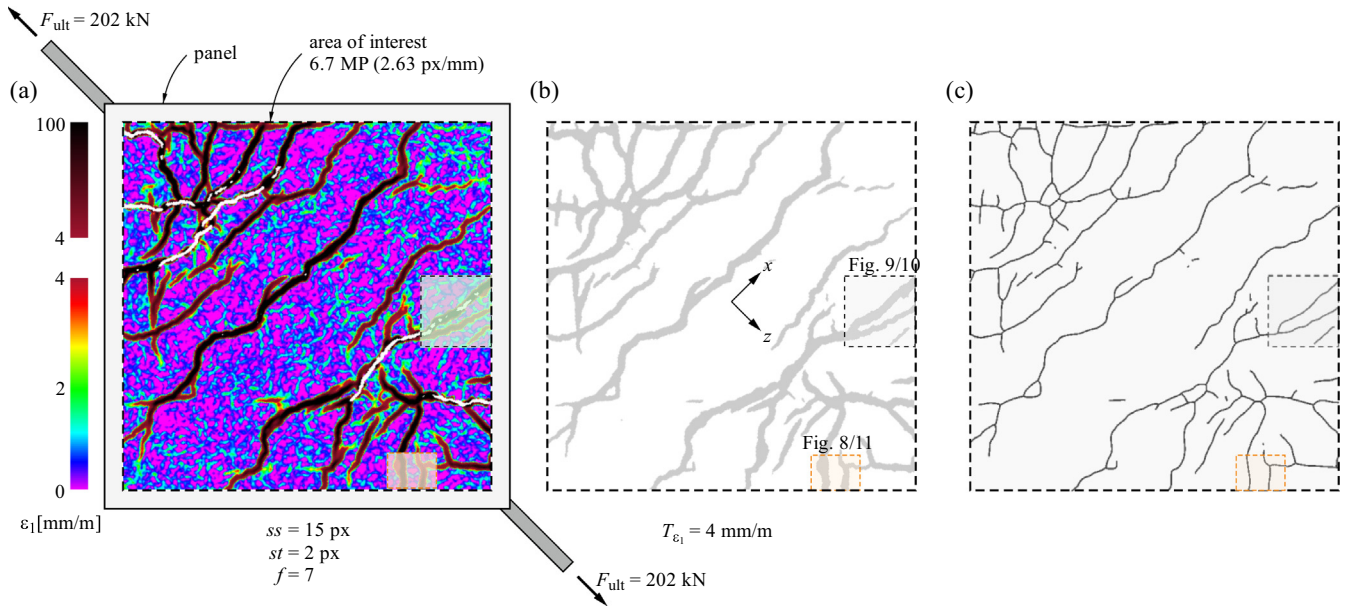
Fig. 7. Crack detection of the reference panel experiment [39] (windows indicate parts of the panel used for uncertainty analyses): (a) principal tensile strain field at ultimate load F_{ult}; (b) high strain areas; (c) smoothed crack line skeleton.

Table 1
Influence of strain filter size f on minimum detectable crack width ($\delta_{n,min}$) and spacing (s_{min}) for the particular case of the reference experiment in Fig. 7.

f	7	15	23	31
s_{min} (Eq. (8))	43.8 px (16.7 mm)	66.5 px (25.3 mm)	89.1 px (33.9 mm)	111.7 px (42.5 mm)
$\delta_{n,min}$ (empirical)	0.05 px (0.02 mm)	0.10 px (0.04 mm)	0.13 px (0.05 mm)	0.18 px (0.07 mm)

analysis has been performed qualitatively by superposing the detected crack patterns to the principal tensile strain field showing excellent agreement (see Fig. 7a and c). However, the challenge is that the strain field cannot properly represent the crack locations in areas with closely spaced or converging cracks. In the following, the performance of the herein presented crack detection procedure is qualitatively evaluated for several DIC processing parameters with the help of test results from the panel experiment described in Section 3.2 and shown in Fig. 2a. In particular, the spatial accuracy of the detected crack intersections and the smallest detectable crack spacing and width are discussed.

Fig. 7a shows the DIC principal tensile strain field ε_1 of the panel at ultimate load F_{ult}. This measuring stage shows a stabilised crack pattern and is therefore suitable for the detection of cracks that are used for the crack kinematic measurement of the entire experiment. When selecting the DIC processing parameters, it should be taken into account that a combination of a small subset, step and strain filter sizes allows computing the strains over a very small distance. Such a configuration provides distinct strain peaks at the cracks, at the cost of typically high noise levels of the strain measurement. As will be shown in the following, this is more beneficial for detecting crack locations accurately than having a more accurate strain field but with less distinct strain peaks. The best crack detection results for this particular case have been found using a DIC subset size ss of 15 px, a step st of 2 px and a strain filter size f of 7 (corresponding to a filter mask of 5.3 × 5.3 mm). The threshold of high strain areas T_{ε_1} in Fig. 7b has been set to 4 mm/m, which is above the sum of the measurement's noise and the elastic tensile strains of the material. In order to handle the correlation losses at high crack widths (white areas in

Fig. 7a), high strain areas of 20 previous measuring stages have been combined, as described in Section 3.3. The obtained crack pattern skeleton in Fig. 7c is smoothed using a moving average crack path filter with span 9. For the cracks lying within the marked windows, detailed sensitivity analyses are performed in the following.

Fig. 8 shows the influence of strain filter size f with respect to the smallest detectable crack spacing. Keeping all other parameters constant, less distinct strain peaks and wider high strain areas along the crack path can be seen when increasing f. Since the DIC subsets and the filter masks are aligned with the xz-coordinates and the investigated cracks have an inclination of about 45° respect to the x-axis, the area of increased strains caused by the cracks can extend over a maximum of $\sqrt{2}((f+1) \cdot st + ss)$. This maximum span is used to define the smallest detectable crack spacing:

$$s_{min} = \sqrt{2} \cdot ((f+1) \cdot st + ss) \tag{8}$$

It should be mentioned, that the factor $\sqrt{2}$ in Eq. (8) is conservative when using a typical filter mask with very little influence of measuring points located at the corners of the filter mask (such as the rotationally symmetric Gaussian filter herein used). Additionally, for high values of T_{ε_1}, the actual span of the detected high strain area might be considerably smaller than the extension estimated with Eq. (8). This can be illustrated with the example given in Fig. 8. In this figure, the two parallel cracks in Section A-Â have a separation of 25 mm. According to the smallest detectable crack spacing given by Eq. (8), these two cracks should not be detectable when using a strain filter size of 15 or higher (see Tab. 1). However, the two cracks are still detectable up to a strain filter size of 23.
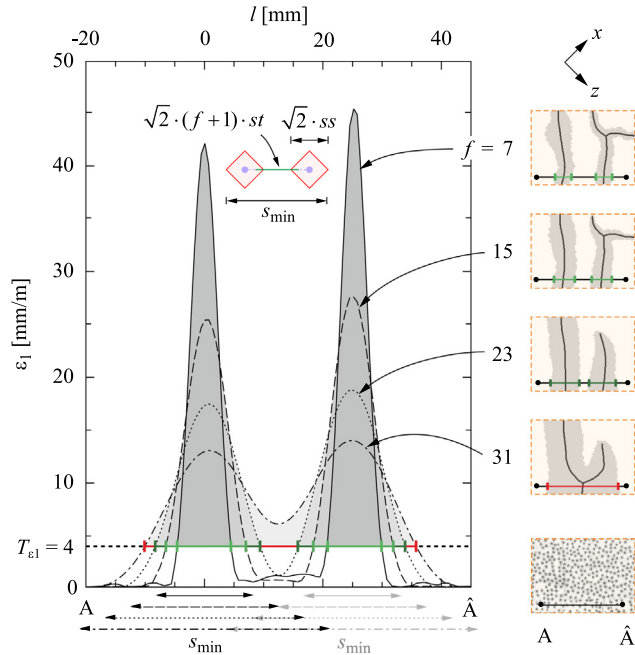
Fig. 8. Influence of strain filter size f on the strain variation across cracks and the smallest detectable crack spacing.

Only for a strain filter size of 31 the high strain areas of the two cracks overlap leading to the detection of a false single crack in the centre of the combined high strain area.

The phenomenon of misinterpreted crack locations can also be observed in the case of converging cracks with similar inclination, shown in Fig. 9. When approaching crack intersections, the crack spacing decreases. Therefore, the localisation of such a point is less accurate when using higher strain filter sizes. A successive shift of the detected crack intersection towards the two converging crack branches can be seen. Using a combination of a small subset, step and strain filter size is highly advantageous for detecting closely spaced cracks and in the precise determination of crack intersections.

The minimum detectable crack width $\delta_{n,\min}$ depends on the DIC parameters as well as on the high strain area threshold T_{ε_1}. In gen-
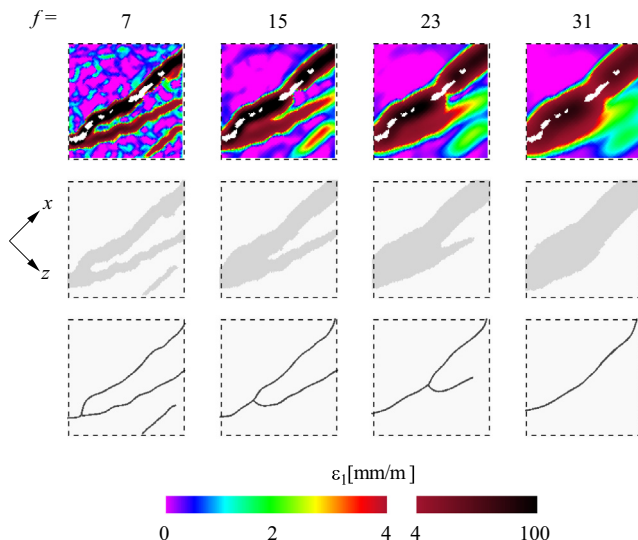
eral, it holds that with lower DIC parameters finer cracks can be detected. This explains the decreasing length of the detected cracks in Figs. 8 and 9 when using higher strain filter sizes. However, defining an analytical expression for the smallest detectable crack width is intricate, as it is affected by the weight functions of the subset and filter mask. For this reason, the values for $\delta_{n,\min}$ denoted in Tab. 1 were empirically obtained. For the DIC configuration used in Fig. 7, cracks with an opening larger than 0.05 pixels (which corresponds to 0.02 mm) are detected, which is significantly below the image resolution. In order to keep the smallest detectable crack width constant when increasing the strain filter size, the high strain area threshold T_{ε_1} would have to be lowered. Such an approach would be feasible due to the reduced noise when using higher strain filter sizes. However, it is usually preferable to proceed with a configuration that includes a low strain filter size allowing precise detection of closely spaced and converging cracks.

4.2. Accuracy of crack inclination

The crack inclination is used on the one hand to define the reference points and on the other hand for the decomposition of the crack displacement vector into crack opening and sliding. As described in Section 3.4, the crack inclination in the undeformed state θ_r^0 is defined by using neighbouring crack points within the crack inclination window of size iw. Fig. 10 shows the influence of the crack shape and the size iw on θ_r^0 and the results for the crack kinematic measurements at the ultimate load state. Three different crack locations (see Fig. 10a, indicated by colour), which differ in their local crack line shape, are analysed for $5 \leqslant iw \leqslant 37$.

In Fig. 10c, it is shown that the size of the crack inclination window can significantly affect the crack inclination θ_r^0: While with $iw = 5$ the crack inclinations of the three investigated locations are parallel to the x-axis, they vary for higher iw, depending on their local crack shape. The green examination point is located at a strong arching part of the crack, leading to significant changes of the crack inclination with increasing iw. In contrast, the crack inclination is only little affected in straight parts of the crack, such as at the orange point. Since the four reference points for the crack kinematic measurements are selected based on θ_r^0 (see Section 3.5), strong changes in crack inclinations cause different reference points being used when varying iw. Such changes of reference points are shown in Fig. 10e, at points where the crack displacement direction $\alpha_r + \theta_r$ jumps. The crack displacement vector slightly varies when using different reference points due to the noise in the DIC measurements. The locations of all used reference points throughout the variation of iw are indicated with black and grey dots in Fig. 10a.

The decomposition of the crack displacement vector into crack opening and sliding (see Fig. 10b and d) depends on the crack inclination. For cracks with a main opening component and moderate changes of θ_r^0, mainly the crack slidings δ_t are affected by the selected value of iw (see Fig. 10d).

4.3. Accuracy of crack kinematic measurements

The accuracy of the crack kinematic measurements depends on the measurement uncertainty of the DIC instrumentation but also on the ability of the measurement procedure presented in Section 3.5 to reproduce the real crack lip displacements. The crack kinematic measurement approach relies on the fundamental assumption of rigid-body displacements at both sides of the crack in the region between the crack lip, the kinematic point, and the rotation point. This can only be guaranteed, if these regions, but also the individual subsets of the reference points, are not disturbed by any discontinuity (i.e. cracks). If these conditions are
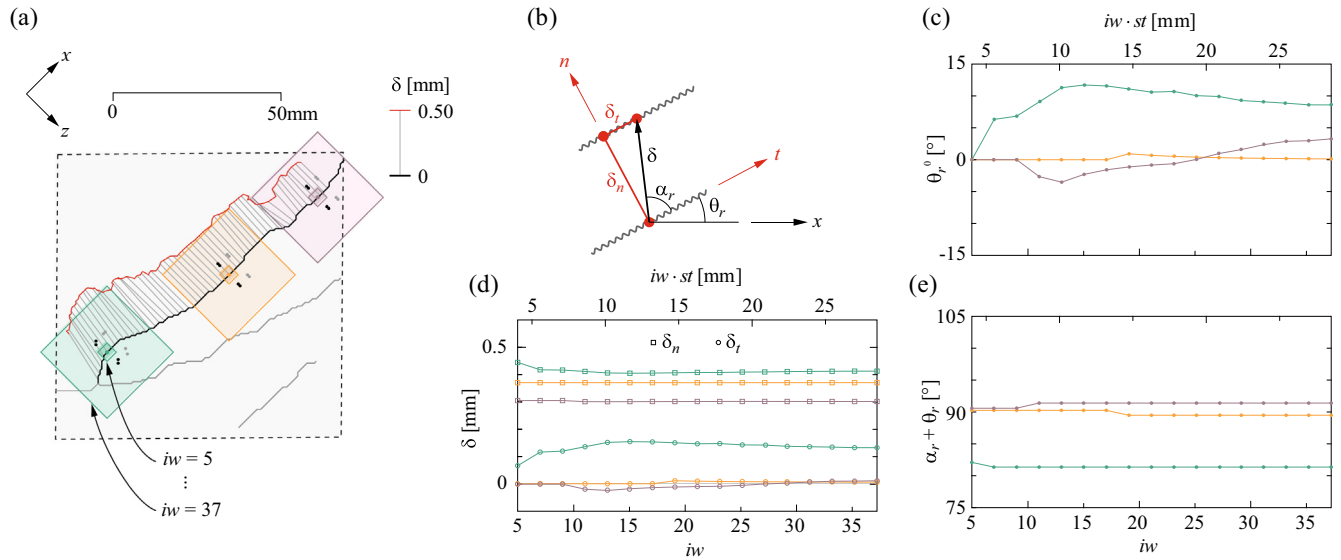

Fig. 9. Influence of strain filter size f on the location of the crack intersection.

Fig. 10. Influence of inclination window size *iw* on crack kinematic measurements: (a) variation of *iw* at three locations (indicated by colour, which is in accord with that of (c), (d) and (e)) with different local crack line shape; (b) decomposition of the crack displacement vector; (c) influence on the crack inclination in the undeformed state θ_r^0; (d) influence on the crack opening δ_n and sliding δ_t measurements; (e) influence on the crack displacement direction.

not satisfied, the calculated crack lip displacements might differ significantly from the actual ones. In order to avoid that the subsets associated to the measuring points intersect the crack to be measured, the minimum separation distance of the kinematic points results in (derived for the critical crack inclination of 45° with respect to the orientation of the subset):

$$d_{1,min} = \sqrt{2} \cdot ss \tag{9}$$

Fig. 11 shows the result of the crack kinematic measurement depending on the separation distance of the two kinematic points
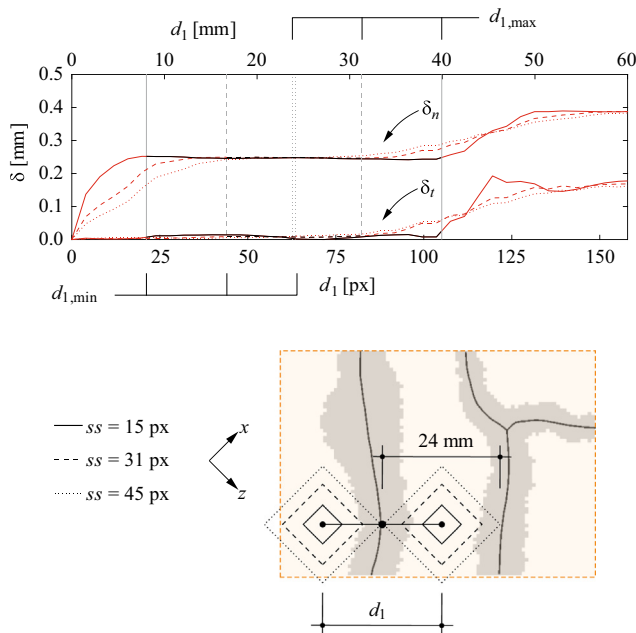

Fig. 11. Sensitivity analysis of the crack kinematic measurement: influence of the separation distance of the two kinematic points d_1 and the subset size *ss* on the crack kinematic measurement (range of reliable results between $d_{1,min}$ (Eq. (9)) and $d_{1,max}$ (Eq. (10)) is marked in black, biased values in red). (For interpretation of the references to colour in this figure legend, the reader is referred to the web version of this article.)

d_1 at a location of almost pure crack opening. The crack location is inclined approximately with the critical angle of 45°. The measurements are conducted for a DIC configuration with step size *st* of 2 and three different subset sizes (15, 31 and 45 px) at ultimate load F_{ult}. It should be mentioned that all crack kinematic measurements shown in Fig. 11 were performed considering a unique crack pattern (detected with *ss* = 15 px and *f* = 7). This allows neglecting the influence of the subset size on the crack location (already discussed in Section 4.1). The separation distance of the rotation points d_2 has been set to the constant value of 20 px (corresponds to 8 mm).

For values of d_1 below the minimum separation distance $d_{1,min}$ according to Eq. (9), the subsets of the kinematic points intersect with the crack. This explains the underestimation of the true crack width δ_n, which is about 0.24 mm. For $d_1 > d_{1,min}$, the crack kinematic measurements remain almost exactly constant at the true value until the subsets intersect with the closely spaced parallel crack at the right side (which contains a significant sliding component). The onset of this influence depends again also on the subset size *ss* and is given by

$$d_{1,max} = 2 \cdot s - \sqrt{2} \cdot ss \tag{10}$$

with *s* being the crack spacing. Biased values are marked in red. In the measurement obtained with *ss* = 15 px, the crack kinematic measurements are thus distorted for d_1 greater than 39.9 mm (part of the kinematics of the adjacent crack are taken into account), which is well shown in Fig. 11. For *ss* = 45 px, there is no plateau at the true crack kinematics, since the minimum separation distance $d_{1,min}$ of 24 mm coincide approximately with the crack spacing (i.e. $d_{1,min} \approx d_{1,max}$). Hence, the applicability of the crack kinematic measurement procedure is limited in the case of closely spaced cracks and thus also in the region of crack intersections. In practical applications, it is proposed to perform the crack kinematic measurement with $d_1 = d_{1,min}$. The use small sparation distances reduces the probability of interferences due to near cracks and keeps the bias caused by the consideration of elastic strains of the material in the crack kinematic measurement as low as possible.

All reliable measurements in Fig. 11 (i.e. $d_{1,min} < d_1 < d_{1,max}$) are marked in black and are very stable. Although in this measuring stage one crack lip is slightly rotated ($\approx 0.1°$ with respect to the
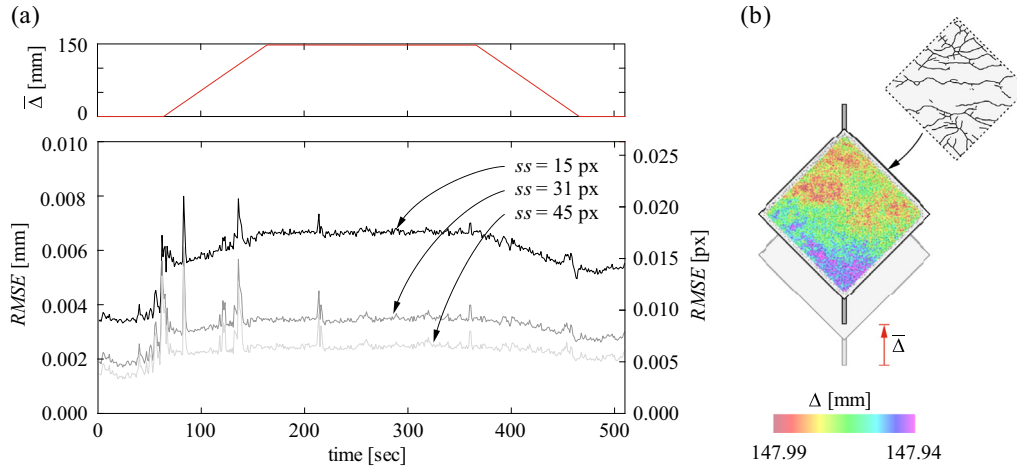
Fig. 12. Zero Strain Test (ZST) according to [9] applied to crack kinematic measurements: (a) root-mean-square error *RMSE* of the crack kinematic measurements (Eq. (11)) for different subset sizes *ss*; (b) specimen at maximum mean displacement $\bar{\Delta}$.

undeformed state), the crack kinematic measurements remain nearly constant for increasing d_1. As discussed in Section 3.5, approaches that do not consider such rotation would provide significantly biased measurements for the crack sliding component (in this example, the incorrect crack sliding component would amount to $\approx 0.001 \cdot d_1$ if crack lip rotations were ignored).

The crack kinematic measurement uncertainty that is linked to the uncertainty of the DIC measurement can be determined by means of a Zero Strain Test (ZST) as proposed in [9] (see Fig. 12). This test is conducted prior to loading by moving the specimen slowly without applying any deformation (rigid-body motion). The obtained measuring series combined with a random but representative crack pattern allows characterising the uncertainty of the crack kinematic measurements. In this case, the final stabilised crack pattern from Fig. 7c was used as representative crack pattern (see Fig. 12b). The root-mean-square error (*RMSE*) of the crack kinematic measurement can be quantified analogously to the uncertainty quantification of general displacement measurements proposed by the Association of German Engineers [48], by the following expression:

$$RMSE = \sqrt{\frac{1}{N} \sum_{q=1}^{N} (\delta_{n,q}{}^2 + \delta_{t,q}{}^2)} \qquad (11)$$

where $\delta_{n,q}$ and $\delta_{t,q}$ denote the measured crack opening and sliding component at each crack point of the applied crack pattern. Fig. 12a shows the *RMSE* of the crack kinematic measurement per measuring stage of the ZST and the mean displacement $\bar{\Delta}$ of the specimen. For this analysis, the measurements were performed using $d_1 = d_2 = d_{1,min}$. The *RMSE* for subset size *ss* = 15 px at maximum mean displacement ($\bar{\Delta} \approx 148$ mm) remain below 0.02 px (which corresponds to 0.008 mm). When using higher subset sizes, the noise level is significantly reduced (in the case of *ss* = 45 px to approximately 0.0025 mm). It should be mentioned that the *RMSE* reflects the global uncertainty over the entire specimen and that the measurement bias can be easily one order of magnitude larger locally (most pronounced at locations far away from the centre of field of view) [9]. In general, the measurement uncertainty increases with the specimen displacement Δ due to inevitable residual imperfections in the system calibration leading to fictitious deformations (see spatial distribution of Δ in Fig. 12b). Thus, a proper calibration is crucial for a high quality of the crack kinematic measurements.

5. Conclusions

The understanding of the crack behaviour is essential in the validation and further development of structural mechanical models for quasi-brittle materials, such as concrete, mortar, or masonry. This paper presents a crack detection and crack kinematic measurement tool that provides a fully automated method for the accurate acquisition and evaluation of the crack behaviour in structural experiments instrumented with digital image correlation (DIC). While conventional crack measurement techniques, such as the visual inspection, demountable mechanical strain gauges or linear displacement sensors only provide spatial discrete information, DIC measurements provide highly accurate quasi-continuous (in time and space) information of surface deformations. In order to exploit the full potential of DIC measurements, the extraction of crack locations and crack kinematics measurements from DIC results is required to be systematic and automated. First attempts into this direction are provided by Mündecke and Mechtcherine [36] and by Ruocci et al. [37,38], with their method being limited to detect individual independent crack points and therefore only applicable to simple crack patterns with non-branching cracks and uniform crack displacement directions in experiments without any rotation.

In the present approach, the crack pattern is extracted as skeleton from DIC results by using well-established methods from image processing. The cracks are detected as thinned traceable lines in areas with principal tensile strains above a certain threshold by applying morphological thinning - showing an excellent agreement with the physical crack pattern. In contrast to direct image-based crack detectors that rely on the variation of pixel intensities of true images, the proposed DIC-based method directly links the detected cracks to the measured surface deformations, thus allowing the extraction of much finer and more reliable cracks. Moreover, the use of principal tensile strains has the advantage that cracks are detected independently of the crack inclination and the crack displacement direction. The comparison to physical crack patterns shows the excellent performance of the crack detector, even with a strain threshold one order of magnitude larger than the maximum elastic tensile strain of the material. Cracks with a minimum opening of 0.05 px (corresponds to 0.02 mm for an image resolution of 0.38 mm/px, which can be obtained in a 2 m field of view using the DIC instrumentation used herein) can be detected. This is up to 100 times smaller than the smallest detectable crack opening of direct image-based crack detection techniques.

The crack kinematic measurement technique uses general formulations in the two-dimensional plane of the investigated surface deformations, thus allowing reliable measurements of full crack kinematics (opening and slip) for any crack inclination. It is conducted at each crack location by tracing the crack path and relying directly on the DIC displacement field. The crack displacement vector in each crack point is obtained with in total four reference points: the crack lip displacements are computed each by two close reference targets assuming a rigid-body displacement in the vicinity of the crack lip. This procedure takes into account local rotations of the specimen, which would otherwise – if the crack kinematics had been characterised using only two reference points – severely biases the results, particularly of crack slidings. The obtained crack displacement vector is decomposed into crack opening and sliding with the help of the local crack inclination – characterised by the local crack line shape - and the mean rotation of both crack lips. The uncertainty of the crack kinematic measurement has been quantified with the help of a Zero Strain Test. For appropriate DIC configurations, it amounts to less than 0.02 px (corresponds to 0.008 mm in the setup used herein), which is more precise by an order of magnitude when compared to direct image-based crack kinematic measurement techniques that rely on the variation of pixel intensities of true images. Moreover, direct image-based methods do not allow for crack slip measurements and are therefore strongly limited in their application.

The main novelty of the proposed procedure in contrast to existing automated crack measurement methods relying on DIC results lies (i) in the application of image processing operations for the extraction of a skeletonized crack pattern with traceable crack lines, and (ii) in the general formulation of the crack kinematic measurement technique, which allows the accurate measurement of a complex crack behaviour in large-scale tests with varying crack inclinations and crack displacement directions and different local rotations of the tested specimen.

While the proposed crack detection and measurement algorithm works perfectly for non-branching and well-separated cracks, it has been shown that the crack detector fails for very closely spaced cracks and in areas near crack intersection due to overlapping high strain areas caused by the individual cracks or crack branches. A more refined crack detector that takes into account the local variations within the high strain area would increase the accuracy of crack locations and avoid the aforementioned problems. Additionally, the identification and removal of spurious unwanted minor crack branches would improve the performance of the crack detector. However, even if the crack locations are extracted very accurately, the crack kinematic measurements at locations with closely spaced cracks and crack intersections may be biased depending on the configuration of reference points. Reliable results can only be obtained if the regions on both crack sides between the crack lip and the reference points move as rigid bodies (i.e. if these points, including their individual DIC subsets are not disturbed by other cracks). The automatic identification of the reliable crack kinematic measurements is not included in the present tool and should be addressed in future works to allow for statistical analyses without the risk of using biased measurements. The use of proper statistical evaluation tools will be essential for the consolidation of the very detailed data provided by the presented tool into more understandable characteristic values, particularly when analysing large-scale experiments.

CRediT authorship contribution statement

Nicola Gehri: Methodology, Software, Writing - original draft, Project administration. **Jaime Mata-Falcón:** Conceptualization, Methodology, Writing - review & editing, Supervision. **Walter Kaufmann:** Conceptualization, Writing - review & editing.

Declaration of Competing Interest

The authors declare that they have no known competing financial interests or personal relationships that could have appeared to influence the work reported in this paper.

References

[1] D. Asprone, C. Menna, F.P. Bos, T.A.M. Salet, J. Mata-Falcón, W. Kaufmann, Rethinking reinforcement for digital fabrication with concrete, Cem. Concr. Res. 112 (2018) 111–121, https://doi.org/10.1016/j.cemconres.2018.05.020.

[2] T. Wangler, N. Roussel, F.P. Bos, T.A.M. Salet, R.J. Flatt, Digital concrete: a review, Cem. Concr. Res. 123 (2019), https://doi.org/10.1016/j.cemconres.2019.105780 105780.

[3] W. Kaufmann, Strength and deformations of structural concrete subjected to in-plane shear and normal forces, doctoral dissertation, Institute of Structural Engineering, ETH Zürich (1998), https://doi.org/10.1007/978-3-0348-7612-4.

[4] F.J. Vecchio, M.P. Collins, The modified compression field theory for reinforced concrete elements subjected to shear, Journal Proceedings 83 (1986) 219–231, https://doi.org/10.14359/10416.

[5] W. Kaufmann, J. Mata-Falcón, A. Amin, Compression field analysis of FRC based on the cracked membrane model, ACI Structural Journal 116 (2019) 213–224, https://doi.org/10.14359/51716763.

[6] T. Markic, A. Amin, W. Kaufmann, T. Pfyl, Strength and deformation capacity of tension and flexural RC members containing steel fibres, ASCE Journal of Structural Engineering 146 (5) (2020), https://doi.org/10.1061/(ASCE)ST.1943-541X.0002614.

[7] Valeri P., Fernández Ruiz M., Muttoni A., New perspectives for design of lightweight structures by using textile reinforced concrete, in: Proceedings of the Fib Symposium 2019, Fédération Internationale du Béton (fib), Kraków, Poland, 2019: pp. 73–80.

[8] Kaufmann W., Mata-Falcón J., BeckA., Future directions for research on shear in structural concrete, in: Fib Bulletin 85: Towards a Rational Understanding of Shear in Beams and Slabs, 2018.

[9] Mata-Falcón J., Haefliger S., Lee M., Galkovski T., Gehri N., Combined application of fibre optic and digital image correlation measurements to structural concrete experiments, Engineering Structures. (submitted).

[10] Presvyri S., Yang Y., Hendriks M., Visser J., Hordijk D., On the extension of walraven's aggregate interlock model based on laser scanned crack surface, in: W. Derkowski, P. Krajewski, P. Gwozdziewicz, M. Pantak, L. Hojdys (Eds.), Proceedings of the Fib Symposium 2019, FIB, 2019: pp. 937–944.

[11] P.B. Morice, G.D. Base, The design and use of a demountable mechanical strain gauge for concrete structures, Mag. Concr. Res. 5 (1953) 37–42, https://doi.org/10.1680/macr.1953.5.13.37.

[12] A. Mohan, S. Poobal, Crack detection using image processing: A critical review and analysis, Alexandria Eng. J. 57 (2018) 787–798, https://doi.org/10.1016/j.aej.2017.01.020.

[13] P. Wang, H. Huang, Comparison analysis on present image-based crack detection methods in concrete structures, in: in: 2010 3rd International Congress on Image and Signal Processing, 2010, pp. 2530–2533, https://doi.org/10.1109/CISP.2010.5647496.

[14] Y.-J. Cha, W. Choi, O. Büyüköztürk, Deep Learning-Based Crack Damage Detection Using Convolutional Neural Networks, Comput.-Aided Civ. Infrastruct. Eng. 32 (2017) 361–378, https://doi.org/10.1111/mice.12263.

[15] E. Cuenca, A. Tejedor, L. Ferrara, A methodology to assess crack-sealing effectiveness of crystalline admixtures under repeated cracking-healing cycles, Constr. Build. Mater. 179 (2018) 619–632, https://doi.org/10.1016/j.conbuildmat.2018.05.261.

[16] M.M.M. Islam, J.-M. Kim, Vision-Based Autonomous Crack Detection of Concrete Structures Using a Fully Convolutional Encoder–Decoder Network, Sensors. 19 (2019) 4251, https://doi.org/10.3390/s19194251.

[17] Y. Li, H. Li, H. Wang, Pixel-wise crack detection using deep local pattern predictor for robot application, Sensors. 18 (2018) 3042, https://doi.org/10.3390/s18093042.

[18] Z. Liu, Y. Cao, Y. Wang, W. Wang, Computer vision-based concrete crack detection using U-net fully convolutional networks, Autom. Constr. 104 (2019) 129–139, https://doi.org/10.1016/j.autcon.2019.04.005.

[19] Q. Luo, B. Ge, Q. Tian, A fast adaptive crack detection algorithm based on a double-edge extraction operator of FSM, Constr. Build. Mater. 204 (2019) 244–254, https://doi.org/10.1016/j.conbuildmat.2019.01.150.

[20] X. Yang, H. Li, Y. Yu, X. Luo, T. Huang, X. Yang, Automatic pixel-level crack detection and measurement using fully convolutional network, Comput.-Aided Civ. Infrastruct. Eng. 33 (2018) 1090–1109, https://doi.org/10.1111/mice.12412.

[21] P. Dare, H. Hanley, C. Fraser, B. Riedel, W. Niemeier, An operational application of automatic feature extraction: the measurement of cracks in concrete structures, Photogram. Rec. 17 (2002) 453–464, https://doi.org/10.1111/0031-868X.00198.

[22] B. Shan, S. Zheng, J. Ou, A stereovision-based crack width detection approach for concrete surface assessment, KSCE J Civ Eng. 20 (2016) 803–812, https://doi.org/10.1007/s12205-015-0461-6.

[23] M.W. Burke, Image Acquisition: Handbook of machine vision engineering: Volume 1, Springer, Netherlands (1996), https://doi.org/10.1007/978-94-009-0069-1.

[24] J.C. Walraven, Aggregate interlock: A theoretical and experimental analysis, Doctoral dissertation, Delft University, 1980.

[25] B. Li, K. Maekawa, H. Okamura, Contact density model for stress transfer across cracks in concrete, J. Faculty Eng., The University of Tokyo. 40 (1989) 9–52.

[26] T. Paulay, P.J. Loeber, Shear Transfer by Aggregate Interlock, ACI Special Publication. SP-42 (1974) 1–16.

[27] F. Cavagnis, M. Fernández Ruiz, A. Muttoni, Shear failures in reinforced concrete members without transverse reinforcement: An analysis of the critical shear crack development on the basis of test results, Eng. Struct. 103 (2015) 157–173, https://doi.org/10.1016/j.engstruct.2015.09.015.

[28] F. Cavagnis, M.F. Ruiz, A. Muttoni, An analysis of the shear-transfer actions in reinforced concrete members without transverse reinforcement based on refined experimental measurements, Structural Concrete. 19 (2018) 49–64, https://doi.org/10.1002/suco.201700145.

[29] P. Huber, T. Huber, J. Kollegger, Investigation of the shear behavior of RC beams on the basis of measured crack kinematics, Eng. Struct. 113 (2016) 41–58, https://doi.org/10.1016/j.engstruct.2016.01.025.

[30] S. Iliopoulos, D.G. Aggelis, L. Pyl, J. Vantomme, P. Van Marcke, E. Coppens, L. Areias, Detection and evaluation of cracks in the concrete buffer of the Belgian Nuclear Waste container using combined NDT techniques, Constr. Build. Mater. 78 (2015) 369–378, https://doi.org/10.1016/j.conbuildmat.2014.12.036.

[31] M. Küntz, M. Jolin, J. Bastien, F. Perez, F. Hild, Digital image correlation analysis of crack behavior in a reinforced concrete beam during a load test, Can. J. Civ. Eng. 33 (2006) 1418–1425, https://doi.org/10.1139/l06-106.

[32] D. Lecompte, J. Vantomme, H. Sol, Crack Detection in a Concrete Beam using Two Different Camera Techniques, Structural Health Monitoring. 5 (2006) 59–68, https://doi.org/10.1177/1475921706057982.

[33] S.Y. Alam, A. Loukili, F. Grondin, Monitoring size effect on crack opening in concrete by digital image correlation, European Journal of Environmental and Civil Engineering. 16 (2012) 818–836, https://doi.org/10.1080/19648189.2012.672211.

[34] S.Y. Alam, A. Loukili, F. Grondin, E. Rozière, Use of the digital image correlation and acoustic emission technique to study the effect of structural size on cracking of reinforced concrete, Eng. Fract. Mech. 143 (2015) 17–31, https://doi.org/10.1016/j.engfracmech.2015.06.038.

[35] M. Muller, E. Toussaint, J.-F. Destrebecq, M. Grédiac, Experimental and numerical study of reinforced concrete specimens strengthened with composite plates, Compos. A Appl. Sci. Manuf. 35 (2004) 885–893, https://doi.org/10.1016/j.compositesa.2004.01.009.

[36] E. Mündecke, V. Mechtcherine, Tensile behaviour of strain-hardening cement-based composites (SHCC) with steel reinforcing bars, Cem. Concr. Compos. 103423 (2019), https://doi.org/10.1016/j.cemconcomp.2019.103423.

[37] G. Ruocci, C. Rospars, P. Bisch, S. Erlicher, G. Moreau, Cracks distance and width in reinforced concrete membranes: experimental results from cyclic loading histories, in: 15th World Conference on Earthquake Engineering, Lisbon, Portugal, 2012: pp. 1278–1284.

[38] G. Ruocci, C. Rospars, G. Moreau, P. Bisch, S. Erlicher, A. Delaplace, J.-M. Henault, Digital Image Correlation and Noise-filtering Approach for the Cracking Assessment of Massive Reinforced Concrete Structures, Strain 52 (2016) 503–521, https://doi.org/10.1111/str.12192.

[39] S. Haefliger, J. Mata-Falcón, W. Kaufmann, Application of distributed optical measurements to structural concrete experiments, in: SMAR 2017 Proceedings, ETH Zurich, 2017.

[40] Correlated Solutions, Vic-3D Software Manual, Correlated Solutions Inc., 2019. http://www.correlatedsolutions.com/supportcontent/VIC-3D-8-Manual.pdf.

[41] M.A. Sutton, J.J. Orteu, H. Schreier, Image Correlation for Shape, Motion and Deformation Measurements: Basic Concepts, Theory and Applications, Springer, US, 2009. https://www.springer.com/gp/book/9780387787466 (accessed August 6, 2019).

[42] P. Reu, Introduction to Digital Image Correlation: Best Practices and Applications, Exp. Tech. 36 (2012) 3–4, https://doi.org/10.1111/j.1747-1567.2011.00798.x.

[43] Correlated Solutions, Strain Calculation in Vic-3D, (2016). http://www.correlatedsolutions.com/supportcontent/strain.pdf (accessed January 24, 2020).

[44] The MathWorks, Inc., Image Processing Toolbox: Reference (2019b), 2019. https://ch.mathworks.com/help/pdf_doc/images/images_ref.pdf (accessed November 25, 2019).

[45] Gambarova P., Karakoç C., A new approach to the analysis of the confinement role in regularly cracked concrete elements, in: International Association for Structural Mechanics in Reactor Technology (Ed.), Transactions of the 7th International Conference on Structural Mechanics in Reactor Technology, Chicago, Illinois, U.S.A., August 22 - 26, 1983. Vol. M: Reliability and Risk Analysis of Nuclear Power Plants, North-Holland Physics Publ, Amsterdam, 1983: pp. 251–261.

[46] S. Campana, M. Fernández Ruiz, A. Anastasi, A. Muttoni, Analysis of shear-transfer actions on one-way RC members based on measured cracking pattern and failure kinematics, Mag. Concr. Res. 65 (2013) 386–404, https://doi.org/10.1680/macr.12.00142.

[47] H. Abdulrahman, B. Magnier, P. Montesinos, From contours to ground truth: how to evaluate edge detectors by filtering, J. WSCG. 25 (2017) 133–142.

[48] Fachbereich Prozessmesstechnik und Strukturanalyse, VDI/VDE 2626 Part 1 - Optical measuring procedures - Digital image correlation - Basics, acceptance test, and interim check, VDI/VDE Gesellschaft Mess- und Automatisierungstechnik, 2018.